Matthias Bleckmann

Itinerant to localized views on *f*-electron systems: A multiprobe study

Cuvillier Verlag Göttingen
Internationaler wissenschaftlicher Fachverlag

Itinerant to localized views on f-electron systems: A multiprobe study

Von der Fakultät für
Elektrotechnik, Informationstechnik, Physik
der Technischen Universität Carolo-Wilhelmina
zu Braunschweig

zur Erlangung des Grades eines
Doktors der Naturwissenschaften
(Dr. rer. nat.)

genehmigte

D i s s e r t a t i o n

von

Matthias Bleckmann

aus Herford

Bibliografische Information der Deutschen Nationalbibliothek
Die Deutsche Nationalbibliothek verzeichnet diese Publikation in der Deutschen Nationalbibliografie; detaillierte bibliografische Daten sind im Internet über http://dnb.ddb.de abrufbar.
1. Aufl. - Göttingen : Cuvillier, 2009
Zugl.: (TU) Braunschweig, Univ., Diss., 2009

978-3-86727-952-9

1. Referent: Prof. Dr. Stefan Süllow
2. Referent: Prof. Dr. Andreas Eichler

eingereicht am: 16. Januar 2009

mündliche Prüfung (Disputation) am: 3. April 2009

Nonnenstieg 8, 37075 Göttingen
Telefon: 0551-54724-0
Telefax: 0551-54724-21
www.cuvillier.de

1. Auflage, 2009
Gedruckt auf säurefreiem Papier

978-3-86727-952-9

Vorabveröffentlichungen der Dissertation

Teilergebnisse aus dieser Arbeit wurden mit Genehmigung der Fakultät für Elektrotechnik, Informationstechnik, Physik, vertreten durch den Betreuer der Arbeit, in folgenden Beiträgen veröffentlicht:

Publikationen:

• M. Bleckmann, O. Prokhnenko, K. Gofryk, D. Kaczorowski, and S. Süllow: *Structural properties of the heavy fermion antiferromagnet UPd_2Sb*, J. Magn. Magn. Mat., **316** (2007) e435.

• M. Bleckmann, A. Buchsteiner, N. Stüßer, K. Gofryk, D. Kaczorowski, and S. Süllow: *Antiferromagnetic structure of UPd_2Sb*, Physica B, in print.

Tagungsbeiträge:

• Joint European Magnetic Symposia (JEMS) 2006 in San Sebastian, Spanien: *Structural properties of the heavy fermion antiferromagnet UPd_2Sb* (Poster).

• Frühjahrstagung der Deutschen Physikalischen Gesellschaft 2007 in Regensburg: *Structural properties of PrB_6* (Poster).

• Magnetic Fields for Science 2007 in Cargese, Frankreich: *The effect of disorder in the heavy fermion compound UPt_2Si_2*(Vortrag).

• International Conference on Strongly Correlated Electron Systems (SCES) 2008 in Buzios, Brasilien: *Antiferromagnetic structure of UPd_2Sb* (Poster).

Contents

List of Figures VII

1 Introduction 1

2 Fundamentals of heavy fermion systems 5
2.1 Heavy fermion systems 5
2.2 Fermi liquid and non-Fermi liquid theory 8
2.3 Quadrupolar ordering 10

3 A case study: Basic properties of $CePt_3B$ 13
3.1 Basic properties of $CePt_3B$ 13
3.2 Bulk methods 16
3.2.1 Magnetization 16
3.2.2 Resistivity 21
3.2.3 Hall effect 29
3.2.4 Specific Heat 33
3.3 Microscopic Methods 38
3.3.1 Neutron scattering 38
3.3.2 μSR measurements 46
3.4 Conclusion of the investigation of $CePt_3B_{1-x}Si_x$ 51
3.4.1 X-ray resonant scattering 52

4 Disorder effects in UPd_2X, X=Sb, Sn 57
4.1 Introduction 57
4.1.1 Review of the class of compounds: UT_2M 58
4.2 Structural and magnetic properties of UPd_2Sb 63
4.2.1 Crystal structure 64
4.2.2 Transport properties 64
4.2.3 Thermodynamic properties 65

4.2.4 Neutron scattering experiments 68
4.2.5 Conclusion 78
4.3 Fermi liquid state in UPd_2Sn 78
4.3.1 Introduction 78
4.3.2 Specific resistivity of $UPd_{2-x}Sn$ 80
4.3.3 Hall effect in UPd_2Sn 88
4.3.4 Conclusion 92

5 UPt_2Si_2: Field induced phases in an antiferromagnet 93
5.1 Introduction 93
5.2 Crystallographic structure 93
5.3 Magnetic properties 97
5.4 Electronic transport properties 103
5.5 High magnetic field measurements 108
5.6 Conclusion 122

6 Ground state properties of $U(Pd_{1-x}Pt_x)_3$ 127
6.1 Introduction 127
6.2 UPd_3: An archetypical quadrupolar ordered system 128
6.3 Bulk properties of $U(Pd_{1-x}Pt_x)_3$ 133
6.3.1 Specific heat 133
6.3.2 Resistivity 137
6.3.3 Susceptibility 141
6.4 Conclusion 145

7 Quadrupolar *vs.* magnetic order in PrB_6 151
7.1 Introduction 151
7.2 Experimental Methods 154
7.3 Experimental Results 155
7.3.1 Structural lattice distortion 155
7.3.2 Charge peaks 163
7.3.3 Magnetic peaks 166

8 Summary 173

Bibliography 177

List of Figures

2.1 Doniach phase diagram 8
2.2 Doniach phase diagram, two alternative scenario 11

3.1 Crystal structure of $CePt_3B$ and $CePt_3Si$ 15
3.2 Inverse susceptibility of $CePt_3B$ 19
3.3 Inverse susceptibility of $CePt_3B$ 20
3.4 Inverse susceptibility of $CePt_3B_{1-x}Si_x$ 21
3.5 Low temperature inverse susceptibility χ^{-1} of $CePt_3B_{1-x}Si_x$. 22
3.6 Magnetization of $CePt_3B$ 23
3.7 Ordered magnetic moment of $CePt_3B$ 24
3.8 Magnetization of $CePt_3B_{1-x}Si_x$ 25
3.9 Temperature dependence of the resistivity of $CePt_3B_{1-x}Si_x$ . . 28
3.10 Temperature dependence of the resistivity of $CePt_3B_{1-x}Si_x$ . . 29
3.11 Normalized resistivity of $CePt_3B_{1-x}Si_x$ 30
3.12 Temperature dependence of $d^2(\rho/\rho_{300})/dT^2$ of $CePt_3B_{1-x}Si_x$. 31
3.13 Phase diagram of $CePt_3B_{1-x}Si_x$ 32
3.14 Hall effect in heavy fermion compounds: Fert and Levy 33
3.15 Specific heat of $CePt_3B$ and $LaPt_3B$ 37
3.16 Structural refinement of $CePt_3B$ 42
3.17 Neutron scattering pattern of $CePt_3B$ 44
3.18 Neutron scattering pattern of $CePt_3B$ 45
3.19 Neutron scattering pattern of $CePt_3B$ 46
3.20 Ferromagnetic simulation of $CePt_3B$ 47
3.21 Antiferromagnetic simulation of $CePt_3B$ 48
3.22 μSR experimental setup 49
3.23 Angular dependence of the μ^+ decay 50
3.24 μ spin polarization of $CePt_3B$ 51
3.25 μSR frequency and χ^{-1} of $CePt_3B$ 52

3.26 Vertical scattering geometry for x-ray scattering 54

4.1 Heusler and $Pnma$ structure 58
4.2 Crystal structure of UT_2M compounds 62
4.3 Electrical resistivity of UPd_2Sb 65
4.4 Inverse magnetic susceptibility of UPd_2Sb 66
4.5 Specific heat of UPd_2Sb 68
4.6 Neutron diffraction pattern of UPd_2Sb at 60 K 70
4.7 Neutron diffraction pattern of UPd_2Sb at 300 K 72
4.8 Detailed view on the (2 2 0) peak of UPd_2Sb 73
4.9 Neutron diffraction pattern of UPd_2Sb at 1.6 K and 60 K . . . 75
4.10 Temperature dependence of two peaks of UPd_2Sb 76
4.11 Ordered magnetic moment of UPd_2Sb from neutron diffraction 77
4.12 Peak width of a magnetic and a structural peak of UPd_2Sb . . 79
4.13 Resistivity of UPd_2Sn 82
4.14 Resistivity of $UPd_{1.98}Sn$ 83
4.15 Resistivity of $UPd_{1.96}Sn$ 84
4.16 Resistivity of $UPd_{2-x}Sn$ 85
4.17 Normalized resistivity of $UPd_{2-x}Sn$ 86
4.18 Fit quality versus $T(N)$ for UPd_2Sn 87
4.19 Fermi liquid temperature versus ρ_{300}/ρ_0 for $UPd_{2-x}Sn$ 89
4.20 Hall coefficient of $UPd_{2-x}Sn$ 90
4.21 Normalized Hall coefficient of $UPd_{2-x}Sn$ 91

5.1 The tetragonal structures of $CaBe_2Ge_2$ and $ThCr_2Si_2$ 94
5.2 Thermal displacement in UPt_2Si_2 97
5.3 Lattice parameter of UPt_2Si_2 98
5.4 Susceptibility χ of UPt_2Si_2 99
5.5 Susceptibility χ of UPt_2Si_2 100
5.6 Specific heat c_{p} of UPt_2Si_2 101
5.7 Magnetic specific heat $c_{\mathrm{p,mag}}$ of UPt_2Si_2 101
5.8 Linewidth of (1 0 0) Bragg peak of UPt_2Si_2 102
5.9 Temperature dependence of the resistivity ρ of UPt_2Si_2 104
5.10 Temperature dependency of the resistivity ρ of UPt_2Si_2 105
5.11 Temperature dependency of $d\rho/dT$ of UPt_2Si_2 106
5.12 Spin gap Δ and T_N of UPt_2Si_2 107

5.13 High field magnetization of UPt_2Si_2 for $B//a$ 109
5.14 High field magnetization of UPt_2Si_2 for $B//c$ 110
5.15 Measured *vs.* calculated high field magnetization of UPt_2Si_2 . 111
5.16 High field magnetization of UPt_2Si_2 for $B//a$ 112
5.17 High field magnetization of UPt_2Si_2 for $B//c$ 113
5.18 High magnetic field susceptibility of UPt_2Si_2 for $B//a$ 114
5.19 High magnetic field susceptibility of UPt_2Si_2 for $B//c$ 115
5.20 High magnetic field resistivity of UPt_2Si_2 for $B//a$ 116
5.21 High magnetic field resistivity of UPt_2Si_2 for $B//c$ 117
5.22 High magnetic field resistivity of UPt_2Si_2 for $B//a$ 118
5.23 High magnetic field resistivity of UPt_2Si_2 for $B//c$ 119
5.24 High field resistivity/susceptibility of UPt_2Si_2 for $B//a$ 120
5.25 High field resistivity/susceptibility of UPt_2Si_2 for $B//a$ 121
5.26 High field resistivity/susceptibility of UPt_2Si_2 for $B//c$ 122
5.27 High field resistivity/susceptibility of UPt_2Si_2 for $B//c$ 123
5.28 Magnetic phase diagram $B//a$ of UPt_2Si_2 124
5.29 Magnetic phase diagram $B//c$ of UPt_2Si_2 125
5.30 Magnetic phase diagram $B//c$ of URu_2Si_2 126

6.1 Double hexagonal structure of UPd_3 129
6.2 Crystallographic A plane in the UPd_3 lattice 130
6.3 Antiferroquadrupolar structure of UPd_3 130
6.4 Phase diagram of $U_{1-x}Np_xPd_3$ 131
6.5 Phase diagram of $U(Pt_{1-y}Pd_y)_3$ 132
6.6 Specific heat of $U(Pd_{1-x}Pt_x)_3$ with $x = 0.005; 0.01$ 134
6.7 Specific heat of $U(Pd_{1-x}Pt_x)_3$ with $x = 0; 0.005$ and 0.01 . . . 135
6.8 Magnetic entropy of $U(Pd_{1-x}Pt_x)_3$ with $x = 0$, 0.005 and 0.01 136
6.9 Magnetic entropy of $U(Pd_{1-x}Pt_x)_3$ with $x = 0; 0.005$ and 0.01 137
6.10 Specific heat of $U(Pd_{1-x}Pt_x)_3$ with $x = 0.005$ 138
6.11 Temperature dependence of ρ and $d\rho/dT$ of $U(Pd_{1-x}Pt_x)_3$ . . 139
6.12 Temperature dependence of ρ of $U(Pd_{1-x}Pt_x)_3$ 140
6.13 Temperature dependence of $d\rho/dT$ and $c_{\mathrm{p,mag}}$ of $U(Pd_{1-x}Pt_x)_3$ 141
6.14 $1/Td\rho/dT$ and $d^2\rho/dT^2$ of $U(Pd_{1-x}Pt_x)_3$ 142
6.15 Susceptibility $B//a$ of $U(Pd_{1-x}Pt_x)_3$ with $x = 0.005; 0.01$ . . 143
6.16 Susceptibility $B//c$ of $U(Pd_{1-x}Pt_x)_3$ with $x = 0.005; 0.01$ . . 144
6.17 Low T susceptibility of $U(Pd_{1-x}Pt_x)_3$, $x = 0.005; 0.01$ 145

6.18 ZFC-FC splitting of U($Pd_{1-x}Pt_x$)$_3$, $x = 0.005$ for $B//a$ 146
6.19 ZFC-FC splitting of U($Pd_{1-x}Pt_x$)$_3$, $x = 0.005$ for $B//c$ 147
6.20 Phase diagram of U($Pd_{1-x}Pt_x$)$_3$ 148
6.21 Magnetic phase diagram of U($Pd_{1-x}Pt_x$)$_3$, for $x = 0.005$. . . . 149

7.1 Crystal structure of PrB_6 152
7.2 Magnetic structure of PrB_6 153
7.3 Accessible and investigated reflections 155
7.4 In plane and out of plane mesh scans on PrB_6 at 5.5 K 156
7.5 In plane and out of plane mesh scans on PrB_6 at 1.7 K 157
7.6 In plane scan of the (2 2 2) peak of PrB_6 158
7.7 Typical scan of the (1 1 0) peak of PrB_6 159
7.8 T dependence of the (1 1 0) peak of PrB_6 160
7.9 Hysteresis of the (1 1 0) Bragg peak of PrB_6 161
7.10 Distortion from cubic to rhombohedral system. 162
7.11 Energy scan of (3/2 3/2 0) 163
7.12 k dependent scans of (3/2 3/2 0) 164
7.13 T dependence of (3/2 3/2 0) 165
7.14 Energy scans of the (5/4 5/4 1/2) peak at $T = 1.7$ K 166
7.15 Temperature dependence of the (7/4 7/4 1/2) peak 168
7.16 Azimuthal scans of the (5/4 5/4 1/2) reflection 169
7.17 Azimuthal scans of the (7/4 7/4-δ 1/2) reflection 170
7.18 Azimuthal scans of the (3/4 5/4 -1/2) reflection 171

1 Introduction

Nowadays, many modern materials, such as high-temperature superconductors, geometrically frustrated oxides and low-dimensional magnets, are discussed in terms of strong correlations in complex systems. Common to these materials is that their unique properties arise from many-body effects. In particular, in this field strongly correlated electron materials represent one of the major topics. Here, to obtain more insight in this - on behalf of theory - still poorly understood research area, model systems are needed in order to advance our knowledge on correlated electron materials in particular and correlation physics in general. In this situation, the physics of heavy fermion systems, as archetypical strongly correlated electron systems, is one key to better understand such behavior.

As a result of electronic correlations, heavy fermion systems display a wide range of exotic features, such as

- quantum phase transitions and non-Fermi liquid behavior, *e.g.* in $CeCu_{5.9}Au_{0.1}$ [1–5];
- unconventional superconductivity, *e.g.* in UPt_3 [6];
- "hidden order" phases, as observed in URu_2Si_2 [7].

Inherent to heavy fermions is the vicinity to a magnetic instability as a result of the hybridization J between conduction and localized f electrons. The physical ground state properties of heavy fermions as function of the strength of hybridization is schematically summarized in the so-called Doniach phase diagram. With decreasing hybridization these materials transform from an intermediate valence state for large J values into a stable f-shell system, and in between crossing the Kondo regime. In the Kondo regime, the hybridization between conduction and f-electrons is the source for strong correlations between the electrons. As long as no magnetic order occurs, this behavior can be described in terms of Fermi liquid behavior.

Upon further reduction of the hybridization, at a critical hybridization value J_c magnetic order sets in. At J_c the physics of heavy fermion systems is determined by quantum fluctuations, hence the name quantum critical point (QCP). At the QCP exceptional physical properties are observed, such as non-Fermi liquid behavior with a resistivity deviating from Fermi liquid behavior. Experimentally, in most cases magnetically ordered heavy fermion system can be tuned by external control parameters such as pressure or magnetic fields through such a quantum critical point.

On the low hybridization side of the Doniach phase diagram are systems with localized f-electrons. These f-electrons can potentially order, resulting in magnetically ordered structures composed of dipolar moments. Further, higher multipole moments, in particular quadrupolar moments, can also exhibit ordered structures and control the physical ground state properties.

One of the main open topics concerning heavy fermions is the interplay between crystallographic disorder and the correlated electron state. Enhanced disorder effects are arising from correlations between the charge carriers. Furthermore, non-Fermi liquid behavior is predicted and observed for moderately structural disordered systems in the vicinity of a quantum critical point.

In contrast, for strongly localized or completely delocalized systems pronounced disorder effects are not expected. An investigation of the effect of disorder on the degree of itinerancy appears to be of interest. Therefore, in this thesis materials with a varying level of itinerancy are investigated with respect to the physical ground state properties. In particular, materials studied here are ranging from Ce intermetallics like $CePt_3B$, U heavy fermion systems such as UPd_2Sb, and UPd_2Sn, or systems previously considered to be strongly localized, *viz*., UPt_2Si_2 and UPd_3. Finally, a truly localized f-electron material, PrB_6, is studied regarding its properties.

The outline of this thesis is as follows:

In **Chapter 2** a brief introduction in the theory of heavy fermion systems is provided. The competition between magnetic RKKY interaction and Kondo interaction is summarized in the Doniach phase diagram. The properties of the Fermi liquid model are summarized and concepts accounting for non-Fermi liquid behavior are pointed out. Finally, a brief introduction into quadrupolar ordering will be provided.

In **Chapter 3** the experimental methods used in this thesis are described and illustrated using measurements on the alloying series $CePt_3B_{1-x}Si_x$. Bulk property studies from previous works, in particular susceptibility, specific heat and electronic transport, on $CePt_3B$ reveal a first transition into an antiferromagnetic and secondly at lower temperatures into a weak ferromagnetic phase. In addition, here the bulk properties of the alloyed samples $CePt_3B_{0.8}Si_{0.2}$ and $CePt_3B_{0.6}Si_{0.4}$ have been investigated. Using these measurements the phase diagram of $CePt_3B_{1-x}Si_x$ has been generated. In order to verify the scenario deduced from the bulk property study and to determine the magnetic structure neutron scattering experiments on $CePt_3B$ have been carried out. Surprisingly, in our neutron scattering experiments no evidence of neither antiferromagnetic nor ferromagnetic order has been found. Subsequently, μSR measurements have been carried out to successfully prove the existence of bulk magnetism in $CePt_3B$. In addition, at the end of Chapter 3 an introduction into resonant x-ray scattering is given to provide the basis for the experiments presented on PrB_6.

In **Chapter 4** two closely related material classes are investigated, namely UPd_2Sb and $UPd_{2-x}Sn$. First, a review of the properties of the Heusler compounds UT_2M (T: d electron element, M heavier element such as In, Sn Sb or Pb) investigated so far is presented. In the following, the heavy fermion system UPd_2Sb is investigated by means of neutron scattering experiments. From these data, it is shown that unconventional semi-conductor like behavior of the resistivity can be accounted for by structurally disordered regions in the sample. The antiferromagnetic structure has been determined and the neutron scattering experiments reveal an interplay of structural disorder and magnetism. The influence of structural disorder on the Fermi liquid properties has been investigated on a series of compounds $UPd_{2-x}Sn$, with different stoichiometric composition ($x = 0$, 0.02 and 0.04) and different heat treatments. Using these experimental results the predictions on disorder induced non-Fermi liquid behavior in the vicinity of a quantum critical point and the influence of structural disorder on the Hall effect have been investigated.

Chapter 5 is dedicated to the moderately mass enhanced compound UPt_2Si_2. Previously, UPt_2Si_2 has been discussed as a local moment antiferromagnet, which ought to be describable by a crystal electric field level scheme. In our reinvestigation of the low temperature electronic transport properties strong

evidence has been found, that UPt_2Si_2 is better understood in terms of an itinerant system rather than a localized one. This evidence of delocalized f-electron behavior has been supported by susceptibility and resistivity measurements in high magnetic fields. Furthermore, a new phase diagram, based on high magnetic field magnetization and resistivity measurements, has been generated and new field induced phases have been observed. Altogether, these findings imply that UPt_2Si_2 has to be discussed as a delocalized f-electron system with the unusual physical properties arising from Fermi surface effects.

Chapter 6 discusses the influence of Pt doping on the properties of antiferroquadrupolar ordered intermetallic UPd_3. The phase diagram of $U(Pd_{1-x}Pt_x)_3$ has been generated by means of specific heat, electronic transport and susceptibility measurements. We show that UPd_3 is very sensitive to Pt doping, *i.e.*, a very small amount of Pt in UPd_3 destroys the quadrupolar ordered phases. Moreover, the magnetic phase diagram of $U(Pd_{1-x}Pt_x)_3$, $x = 0.005$, has been obtained by means of susceptibility and resistivity measurements in different applied magnetic fields. Furthermore, a newly observed splitting in the susceptibility between zero-field cooled and field cooled measurements with the magnetic field applied along the crystallographic c-axis is detected, which possibly is associated to a quadrupolar and magnetic transition.

In **Chapter 7** the results of a detailed study of the rare earth hexaboride PrB_6 by means of resonant x-ray scattering is presented. PrB_6 undergoes two phase transitions, the first one from a paramagnetic into an incommensurate, antiferromagnetically ordered phase and at lower temperatures a second one into a commensurate antiferromagnetic phase. In this study, structural Bragg peaks are investigated for all three phases and evidence of a lattice distortion in the commensurate phase has been provided. Furthermore, detailed investigations on magnetic and charge Bragg peaks have been carried out. The Bragg peaks associated with charge ordering have been examined in all three phases. In addition, the type of magnetic ordering in the commensurate and incommensurate phase has been determined.

2 Fundamentals of heavy fermion systems

2.1 Heavy fermion systems

Heavy fermion systems represent an archetypical class of strongly correlated electron systems. Most of the heavy fermion systems contain materials with partly filled $4f$- or $5f$-shells like Ce, Yb, U, and Np. Well-known and extensively investigated examples are $CeAl_3$, $CeCu_2Si_2$, UPt_3 or $CeCu_6$ [8–11].

For a characterization of the essential properties of these materials it is useful to distinguish between two temperature regimes with a qualitatively different behavior of the electron system. The transition between these two regimes is not sharp, therefore a temperature T_{co} is introduced as a measure for the crossover between the two regimes.

Above T_{co} the electrons behave like a weakly interacting ensemble of local f-moments and conduction electrons. In contrast, in the low temperature regime the electrons behave like a collection of electrons with strongly enhanced effective mass, the heavy fermion quasiparticles, that scatter one another. For $T < T_{\mathrm{co}}$, such behavior results from the hybridization between the local f-electrons and the delocalized conduction electrons. The strength of this hybridization is given via Fermi's golden rule

$$\Gamma = \pi V^2 N(E_{\mathrm{F}}), \tag{2.1}$$

with $N(E_{\mathrm{F}})$ representing the density of states at the Fermi Energy E_{F}, and V as an average of the hybridization matrix element.

Regarding the hybridization strength Γ three regimes can be distinguished:

- $\Gamma \ll E_0 \rightarrow$ stable $4f$-shell,
- $\Gamma < E_0 \rightarrow$ Kondo regime,
- $\Gamma \geq E_0 \rightarrow$ intermediate valence regime,

where E_0 is the binding energy of an unperturbed f^n state. In the first case, the hybridization is relatively small, and therefore the mixing of localized and delocalized states can be neglected. The magnetic properties can be described using a Heisenberg exchange, taking into account the f-level crystal field splitting induced by the local f-ion symmetry. With a residual magnetic exchange, as a consequence very often long range antiferromagnetic ordering is observed for materials residing in this parameter range.

In the Kondo regime $\Gamma < E_0$, in comparison to the intermediate valence regime $\Gamma \geq E_0$, a stable f-state is present. Hence, only small deviations from an integer valence state of the f-ion can be found. In this range, hybridization between localized and delocalized electrons controls the behavior of the materials. Then, at temperatures below T_{co}, an extremely enhanced Pauli susceptibility appears because of the large effective electron mass, in contrast to the Curie-Weiss behavior occurring for temperatures higher than T_{co}.

In the last case, the intermediate valence regime, a strong mixing of f-electrons and conduction electrons is present. Therefore, the f-states are unstable, with a non-integer valency, resulting in a non-magnetic ground state. Still, in contrast to ordinary metals a typically one order of magnitude enhanced Pauli susceptibility is observed as a result of electronic hybridization.

The label "Kondo" for the second regime derives from the so-called Kondo effect [12]. Originally, it describes a situation in which dilute magnetic moments, embedded in a metallic host matrix, are screened by the conduction electrons of the surrounding matrix below a certain temperature T_{K}. Hence, a non-magnetic singlet ground state, with the singlet consisting of the local moment spin and the oppositely aligned spins of the conduction electron screening cloud, is formed. The tell-tale mark of this kind of singlet formation is an increase of the resistivity at temperatures somewhat below T_{K} with $\rho \propto \ln(T/T_{\mathrm{K}})$ for decreasing temperature, and a resistive saturation at lowest temperatures with $\rho \propto (1 - (T/T_{\mathrm{K}})^2)$ [13].

An equivalent situation is believed to exist in heavy fermions for $\Gamma < E_0$, *i.e.*, in the Kondo regime. In these systems the f-electron atoms reside on a regular sublattice of the crystal structure, hence the label "Kondo lattice". With the hybridization Γ the conduction electrons are coupled to the f-electrons, leading to screening processes analogous to the single ion Kondo effect.

For high temperatures ($T > T_{\mathrm{K}}$) the physical properties of such systems are those of ordinary f-electron local moment systems. Below T_{K}, screening processes develop, yielding a behavior which initially resembles that of the single ion Kondo effect, with for instance a strongly enhanced Pauli susceptibility. Only, as temperature is further lowered, stark deviations from the single impurity Kondo model appear due to phase correlations between the different Kondo scattering centers. With the periodicity of the f electron sublattice the Kondo singlets can form a Bloch wave state, resulting in a decreasing resistivity with decreasing temperature, in contrast to the single impurity model. This low temperature coherent state is well described by Fermi liquid theory.

Further, in contrast to dilute Kondo systems, in a Kondo lattice the interactions between the magnetic moments can no longer be neglected. For f electron systems these interactions are of the Ruderman-Kasuya-Kittel-Yosida (RKKY) type. Within the so-called "Doniach model" [14] the energy scale related to this coupling strength, which promotes long-range magnetic order, is given by

$$k_{\mathrm{B}}T_{\mathrm{RKKY}} \propto |\Gamma N(E_{\mathrm{F}})|^2, \tag{2.2}$$

with k_{B} - Boltzmann factor, T_{RKKY} - temperature characterizing RKKY-exchange strength, E_{F} - Fermi energy, $N(E_{\mathrm{F}})$ - density of states at the Fermi level and Γ - hybridization between conduction and localized electrons.

On the other hand, the Kondo interaction, which tends to suppress magnetic order, has to be taken into account, and for which the corresponding energy scale evolves like

$$k_{\mathrm{B}}T_{\mathrm{K}} \propto \exp\frac{-1}{|\Gamma N(E_{\mathrm{F}})|}, \tag{2.3}$$

with T_{K} - temperature characterizing Kondo coupling.

As a result, there are two competing energy scales, one promoting magnetic order, the other suppressing it. The combined behavior is schematically summarized in the "Doniach phase diagram" (Fig. 2.1) (originally derived within molecular field approximation of the periodic Anderson model for a one dimensional system of $S = 1/2$ spins). As a consequence of the competition there is a critical hybridization value Γ_c, which separates a spin compensated state of strong hybridization with $|\Gamma N(E_{\mathrm{F}})| > |\Gamma_{\mathrm{c}} N(E_{\mathrm{F}})|$ from a weakly hybridized state with magnetic order for $|\Gamma N(E_{\mathrm{F}})| < |\Gamma_{\mathrm{c}} N(E_{\mathrm{F}})|$. Heavy

fermions are located close to the magnetic instability at Γ_c, where the competition between the Kondo and the RKKY interaction is strongest.

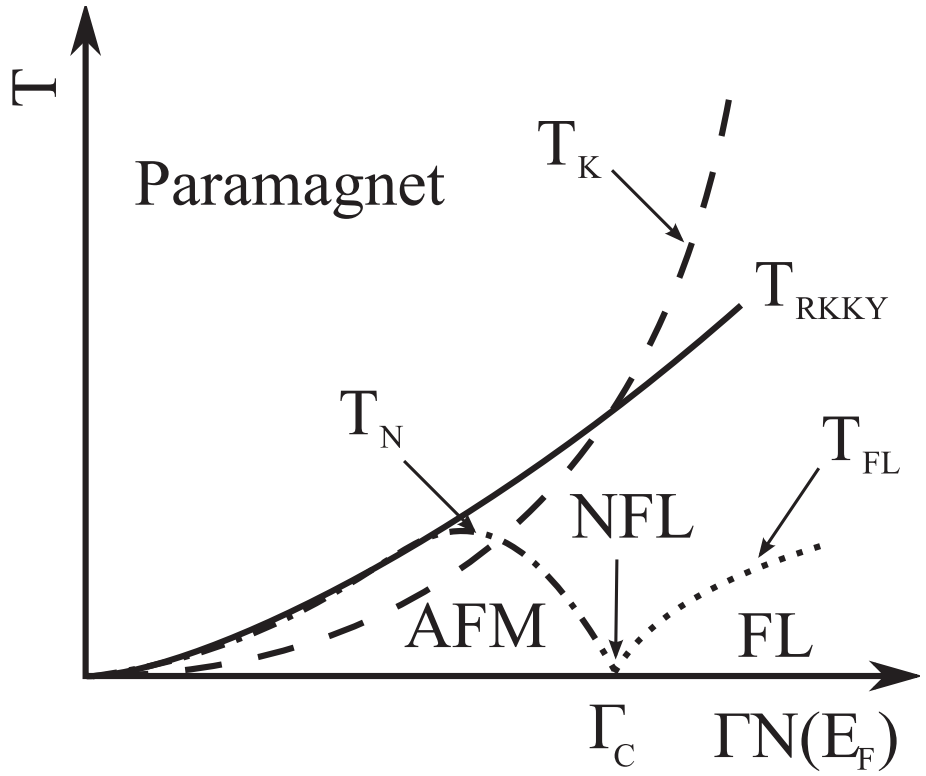

Figure 2.1: The Doniach phase diagram of the one-dimensional Kondo-lattice [15]; for details see text.

2.2 Fermi liquid and non-Fermi liquid theory

In contrast to most common metals where the conduction electrons are considered as independent and non-interacting particles, in strongly correlated electron systems the electron-electron interaction cannot be neglected. In order to deal with this issue, with the Fermi liquid theory the concept of fermionic quasiparticles is introduced. According to energy and momentum conservation and Pauli exclusion principle low energy excitations (*e.g.*, an additional electron at a wave vector $\boldsymbol{k}$ with $|\boldsymbol{k}| = k > k_\mathrm{F}$ and $k - k_\mathrm{F} \ll k_\mathrm{F}$, where k_F is the Fermi wave vector) of the Fermi sea are very stable with a lifetime of $\tau_k \approx (k - k_\mathrm{F})^2$. Furthermore, there is a one-to-one mapping of the

low energy eigenstates of these quasiparticles to the eigenstates of a system of non-interacting electrons. The total energy of a system of weakly excited quasiparticle states with respect to the various occupation numbers of states (with momentum $\boldsymbol{k}$ and spin projection $\sigma = \pm$) is given by

$$E = E_{\mathrm{G}} + \sum_{\boldsymbol{k},\sigma} \epsilon(\boldsymbol{k}) \delta n_{\boldsymbol{k},\sigma} + \sum_{\boldsymbol{k},\sigma;\boldsymbol{k'},\sigma'} f(\boldsymbol{k},\sigma;\boldsymbol{k'},\sigma') \delta n_{\boldsymbol{k},\sigma} \delta n_{\boldsymbol{k'},\sigma'}, \tag{2.4}$$

with E_{G} - ground state energy. $\epsilon(\boldsymbol{k}) \approx v_{\mathrm{F}}(k - k_{\mathrm{F}})$ is the quasiparticle dispersion, which is parameterized by $v_{\mathrm{F}} = k_{\mathrm{F}}/m^*$, where m^* is the effective mass of the quasiparticle. The last term in Eq. 2.4 incorporates the self-interaction among the quasiparticles.

For many heavy fermion systems it has been demonstrated that their properties can be understood within the Fermi liquid theory, with an effective mass m^* which is 2 to 3 orders of magnitude larger than the free electron mass (hence the name "heavy fermions"). However, while the Fermi liquid theory has successfully been applied in the context of heavy fermion physics, in recent years many compounds out of this class of materials have been found which show deviations from Fermi liquid behavior in their basic physical properties, and therefore have attracted a lot of interest. These systems have been labeled non-Fermi liquid systems (commonly abbreviated as NFL systems). Currently, there are various models to account for non-Fermi liquid behavior in f electrons systems, of which the most important ones will be briefly summarized:

- Multichannel Kondo effect: The f electrons are overscreened with more than one conduction electron per f electron site stemming from different conduction bands or channels. The overcompensation gives rise to non-Fermi liquid behavior [16, 17].
- The disordered Kondo model scenario: Because of structural disorder, different f electrons in a system have different Kondo temperatures, resulting in a distribution of Kondo temperatures in this system, this way leading to non-Fermi liquid anomalies in various physical properties [18].
- Griffiths phase model: Similarly, in the Griffiths phase model - as a result of crystallographic disorder - magnetic cluster of different sizes appear in the paramagnetic phase in the proximity to a quantum critical point

(QCP). Magnetic fluctuations associated to these clusters yield non-Fermi liquid behavior [19, 20].

- Vicinity of a quantum critical point: In the vicinity of a QCP the physical properties are determined by excitations generated by quantum fluctuations rather than single fermion excitations, yielding a non-Fermi liquid behavior [21, 22]. In this context, in recent years two different scenarios of the relevant processes have been developed.

  In the first scenario, the spin density wave scenario, the Kondo temperature T_{K} stays finite for all values of an external parameter controlling the ground state. Hence, the local moments are quenched at finite temperatures. The physics close to the QCP is determined by quantum spin fluctuations. In the spin density wave scenario only for a few quasiparticles along "hot lines", which are connected by the ordering vector of the antiferromagnetism $\boldsymbol{Q}$, the inelastic scattering is strong, whereas in the remaining "cold regions" it is weak [23].

  In the second scenario, the local breakdown of the Fermi liquid, the competition between the Kondo effect and the antiferromagnetism leads to a breakdown of the Kondo effect, yielding a suppression of an effective Kondo temperature to $T = 0$. This causes a local destruction of the Fermi liquid at the quantum phase transition, and results in strong scattering over the whole Fermi surface [24].

  Both, the phase diagrams for the spin density wave and local breakdown of the Fermi liquid scenarios are qualitatively depicted in Fig. 2.2 (a) and (b), respectively. $CeCu_{6-x}Au_x$ and $YbRh_2Si_2$ are discussed as materials which display a local breakdown of the Fermi liquid [25, 26], the spin density wave scenario is used to explain the observations in $CePd_2Si_2$, $CeNi_2Ge_2$, and $CeIn_3$ [23, 27–29].

2.3 Quadrupolar ordering

Aside from the Kondo physics at $\Gamma < E_0$, also very stable f electron shells in the limit $\Gamma \ll E_0$ may lead to interesting and exotic phenomena and ground state properties. Especially, in localized f electron systems the ordering cannot only be of dipolar nature (*i.e.*, magnetic), but also higher order multipole